

Research Journal of Pharmaceutical, Biological and Chemical Sciences

A Theoretical Study of the Relationships between Electronic Structure and Antifungal Activity against *Botrytis cinerea* and *Colletotrichum lagenarium* of a Group of Carabrone Hydrazone Derivatives.

Juan S. Gómez-Jeria*.

Quantum Pharmacology Unit, Department of Chemistry, Faculty of Sciences, University of Chile. Las Palmeras 3425, Santiago 7800003, Chile.

ABSTRACT

We present a study of the relationships between the electronic structures of a series of carabrone hydrozone derivatives and their antifungal activities against *Botrytis cinerea* and *Collectotrichum lagenarium*. The electronic structure of all the molecules was obtained using Density Functional Theory at the B3LYP/6-31g(d,p) level. We found statistically significant relationships between the variation of several local atomic reactivity indices and the variation of antifungal activity for the three cases analyzed. The existence of a common skeleton encoding most of the variation of the activity is established for this case. The corresponding antifungal partial pharmacophores are proposed. The *in vivo* and *in vitro* action mechanisms seem to be somewhat different. The method employed here can deal quite well with the σ MOs. A correlation exists between the molecular electrostatic potential structure and the local atomic reactivity indices appearing in the results.

Keywords: Antifungal activity, Carabrone, Common skeleton, Density Functional calculations, Local atomic reactivity indices, QSAR

*Corresponding author

INTRODUCTION

Fungi are essentially important for the successful growth of a large number of plant species, including crops, through the development of mycorrhizal associations. As plants are at the bottom of most food chains, if their growth were restricted all animal life would be seriously reduced through starvation. A number of other fungi are plant parasites. The majority of our common crop plants are vulnerable to fungal attack. Spore production and spreading is extremely efficient in fungi, and plants of the same species growing in fields are prone to extensive attack. Fungal diseases can sometimes result in the loss of whole crops if they are not treated with antifungal agents. These diseases may be controlled with the use of fungicides, but new fungal strains can evolve that are resistant to various agents, and fungicides may be toxic to other organisms. One of the research lines aiming to obtain safer fungicides is to discover antifungal compounds in plants and other living beings. Carabrone (Fig. 1, (3aR,4aS,5S,5aR,6aR)-5a-methyl-3-methylidene-5-(3-oxobutyl)-3a,4,4a,5,6,6a-hexahydrocyclopropa[f][1]benzofuran-2-one) is one of these compounds [1-4].

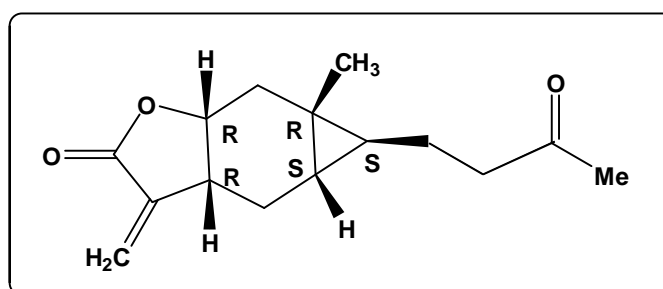


Figure 1. The structure of carabrone. R and S denote the chirality of atomic centers.

Carabrone was first isolated from the fruits of *Carpesium abrotanoides* (Compositae), a biennial herb whose aerial parts have been used in Korean and Chinese medicines to treat bruises and as an insecticide [5, 6]. Carabrone derivatives have antifungal, antibacterial and antitumor activities [7, 8]. Recently, a series of carabrone hydrazones have been synthesized and their antifungal activities evaluated against *Botrytis cinerea* (a necrotrophic fungus that affects many plant species, such as wine grapes, tomatoes, strawberries and bulb crops) and *Colletotrichum lagenarium* (a fungus that targets melons and cucumbers) [9]. We present here the results of a quantum-chemical analysis of the aforesaid compounds with the aim of providing more information about the molecular features involved in their antifungal action.

MODELS, METHODS AND CALCULATIONS.

As the formal model relating structure with biological activity was presented and discussed in many publications we present here only the final result [10-19]. The logarithm of a biological activity (BA) is related to a set of local atomic reactivity indices (LARIs) by the following equation:

$$\begin{aligned} \log(\text{BA}) = & a + \sum_j [e_j Q_j + f_j S_j^E + s_j S_j^N] + \\ & + \sum_j \sum_m [h_j(m) F_j(m) + x_j(m) S_j^E(m)] + \sum_j \sum_{m'} [r_j(m') F_j(m') + t_j(m') S_j^N(m')] + \\ & + \sum_j [g_j \mu_j + k_j \eta_j + o_j \omega_j + z_j \zeta_j + w_j Q_j^{\max}] \end{aligned} \quad (1)$$

where a , e_j , f_j , etc., are constants to be determined. As the definition and physical meaning of the LARIs are well known in quantum chemistry, we shall explain in detail those LARIs appearing in the results. This model was successfully applied to a variety of biological activities [13, 17-42].

The selected molecules were taken from the literature and are shown in Fig. 1 and Table 1.

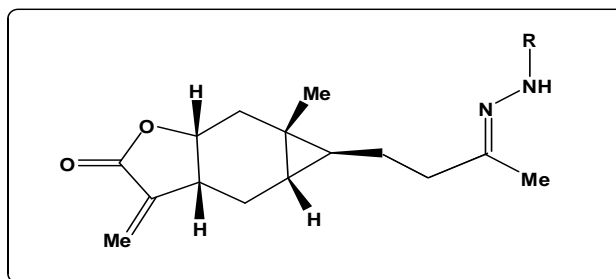
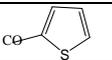
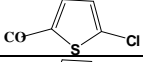
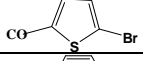
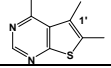


Figure 1. Carabrone hydrazones.

Table 1. Carabrone hidrazones and their antifungal activity.

Mol.	R	log(IC ₅₀) <i>B.cinerea</i> <i>in vitro</i>	log(IC ₅₀) <i>C. lagenarium</i> <i>in vitro</i>	log(IC ₅₀) <i>B.cinerea</i> <i>in vivo</i>
1	COMe	1.43	1.00	1.47
2	COCH ₂ CN	0.98	0.91	0.87
3		0.89	1.03	1.10
4		0.74	0.99	0.98
5		0.68	1.00	0.84
6		0.92	0.31	0.60
7	CO- <i>p</i> -NH ₂ Ph	0.42	0.32	0.68
8	CO- <i>p</i> -OHPh	0.53	0.09	0.67
9	CO- <i>o</i> -OHPh	1.11	0.30	1.12
10	CO- <i>o</i> -ClPh	0.52	0.54	0.98
11	CO- <i>m</i> -ClPh	0.40	0.29	0.94
12	CO- <i>p</i> -NO ₂ Ph	0.53	0.73	0.82
13	CO- <i>p</i> -CNPh	0.39	0.22	0.63
14	CO- <i>m</i> -MePh	0.95	-0.009	1.25
15	CO- <i>p</i> -OMePh	1.01	0.40	1.21
16	CO- <i>m</i> -OMePh	0.80	-0.11	1.09
17	SO ₂ Ph	1.12	0.80	1.24
18	SO ₂ - <i>p</i> -Me-Ph	1.11	0.72	1.23
19	CH ₂ CH ₂ OH	1.23	1.18	1.22
20	Ph	1.21	0.88	1.27
21	2,4,6-tri-Cl-Ph	0.17	0.18	0.32
22	<i>p</i> -nitro-Ph	0.57	0.59	0.66
23	<i>o</i> -nitro-Ph	1.01	0.63	0.95
24	<i>p</i> -CF ₃ -Ph	0.29	0.60	0.74
25	2,3,5,6-tetra-F-Ph	0.10	0.42	0.41
26		1.12	0.21	1.05
27	<i>p</i> -COOH-Ph	1.16	0.84	1.16

The first selected biological activity is the concentration (in µg/mL) of compound inhibiting 50% of spore germination of the fungi *Botrytis cinerea* and *Colletotrichum lagenarium* in an *in vitro* assay. The second selected biological activity was the 50% inhibition of colony growth of *B. cinerea* in mature green tomato fruits (in µg/mL) [9].

Calculations.

The procedure followed here is the same employed in all our recent studies. Briefly, DFT at the B3LYP/6-31g(d,p) level was employed to obtain the electronic structure of the molecules after full geometry optimization with the Gaussian suite of programs [43]. The values of the LARIs were calculated with D-CENT-QSAR software [30]. Negative electron populations arising from Mulliken Population Analysis were corrected

as usual [44]. We assumed that a set of atoms common to the molecules analyzed (common skeleton) encodes the variation of the biological activity throughout the series. We used Linear Multiple Regression Analysis (LMRA) to detect the atoms involved in the variation of the biological activity. The common skeleton is depicted in Fig. 2.

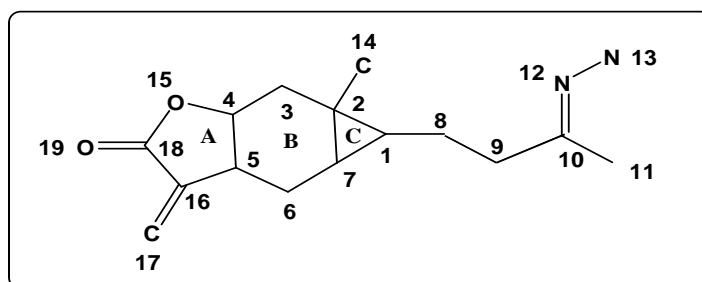


Figure 2. Numbering used for the common skeleton of the carabrone hidrazones.

For the LMRA we built, for each case, a matrix containing the logarithm of the dependent variable ($\log(IC_{50})$) and the local atomic reactivity indices of the atoms of the common skeleton. Statistica software was used for LMRA [45].

RESULTS

We found that there is a high degree of correlation (72%) among the *in vitro* and *in vivo* *Botrytis cinerea* experimental data.

Results for the *in vitro* antifungal activity against *Botrytis cinerea*.

The first LRMA found two outliers. After extracting them we obtained the following statistically significant equation:

$$\log(IC_{50}) = -7.31 - 9.40F_{11}(LUMO)^* - 15.98\omega_{12} + 0.73S_{15}^N - 28.11F_3(HOMO-1)^* + 1.08S_{14}^N(LUMO+1)^* - 3.86F_{15}(HOMO-2)^* \quad (2)$$

with $n=25$, $R=0.94$, $R^2=0.89$, $\text{adj-}R^2=0.86$, $F(6,18)=24.94$ ($p<0.000001$), $\text{outliers}>|2\sigma|=0$ and $SD=0.13$. Here, $F_{11}(LUMO)^*$ is the Fukui index (electron population) of the first vacant MO localized on atom 11, ω_{12} is the electrophilicity of atom 12, S_{15}^N is the total atomic nucleophilic superdelocalizability of atom 15, $F_3(HOMO-1)^*$ is the Fukui index of the second highest MO localized on atom 3, $S_{14}^N(LUMO+1)^*$ is the orbital nucleophilic superdelocalizability of the second lowest vacant MO localized on atom 14 and $F_{15}(HOMO-2)^*$ is the Fukui index of the third occupied MO localized on atom 15. There are no significant correlations between independent variables.

Results for the *in vitro* antifungal activity against *Colletotrichum lagenarium*.

The following statistically significant equation was obtained:

$$\log(IC_{50}) = 2.71 - 30.68F_8(LUMO+1)^* + 3.40F_{11}(HOMO-2)^* - 26.88F_9(LUMO+1)^* + 4.40S_{18}^E(HOMO-1)^* - 13.65\omega_{12} - 0.38F_{10}(LUMO+2)^* \quad (3)$$

with $n=27$, $R=0.97$, $R^2=0.93$, $\text{adj-}R^2=0.91$, $F(6,20)=47.61$ ($p<0.000001$), $\text{outliers}>|2\sigma|=0$ and $SD=0.10$. Here, $F_8(LUMO+1)^*$ is the Fukui index of the second lowest vacant MO localized on atom 8, $F_{11}(HOMO-2)^*$ is the Fukui index of the third highest occupied MO localized on atom 11, $F_9(LUMO+1)^*$ is the Fukui index of the second lowest vacant MO localized on atom 9, $F_{10}(LUMO+2)^*$ is the Fukui index of the third lowest vacant MO localized on atom 10, $S_{18}^E(HOMO-1)^*$ is the local atomic electrophilic superdelocalizability of the second highest occupied MO

localized on atom 18 and ω_{12} is the local atomic electrophilicity of atom 12. There are no significant correlations between independent variables.

Results for the *in vivo* antifungal activity against *Botrytis cinerea*.

The following statistically significant equation was obtained:

$$\log(IC_{50}) = 8.84 - 6.62F_{11}(HOMO)^* - 17.23\omega_{12} - 3.19S_3^E(HOMO-2)^* + 4.64F_{14}(LUMO+2)^* - 5.31Q_7^{\max} - 0.30S_3^N + 0.50S_{15}^E(HOMO-1)^*$$

(4)

with $n=27$, $R=0.92$, $R^2=0.89$, $\text{adj-}R^2=0.85$, $F(7,19)=21.45$ ($p<0.000001$), $\text{outliers}>|2\sigma|=0$ and $SD=0.11$. Here, $F_{11}(HOMO)^*$ is the Fukui index of the highest occupied MO localized on atom 11, $F_{14}(LUMO+2)^*$ is the Fukui index of the third lowest vacant MO localized on atom 14, S_3^N is the total atomic nucleophilic superdelocalizability of atom 3, Q_7^{\max} is the maximal amount of charge atom 7 may receive, ω_{12} is the local atomic electrophilicity of atom 12, $S_3^E(HOMO-2)^*$ is the local atomic electrophilic superdelocalizability of the third highest occupied MO localized on atom 3 and $S_{15}^E(HOMO-1)^*$ is the local atomic electrophilic superdelocalizability of the second highest occupied MO localized on atom 15. There are no significant correlations between independent variables.

DISCUSSION

Figure 3 shows the superimposition of the ten lowest energy conformers of molecule 1 with MarvinView (Dreiding Force Field) [46].

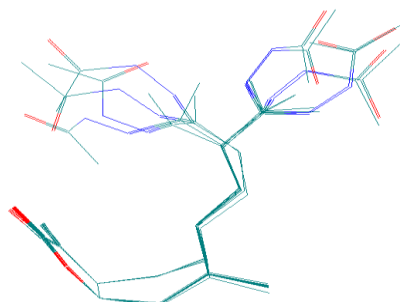


Figure 3. Superimposition of the ten lowest energy conformers of molecule 1.

We can see that in general we may distinguish a group of extended conformers and a group of closed ones. In a living environment or in the laboratory setting where the biological activities were measured, the extended conformers tend to be more stable than the cyclic ones. The latter ones could only become the predominant structure within a highly hydrophobic environment. Figure 4 shows the molecular electrostatic potential (MEP) map of molecule 1 in its fully optimized geometry [47].

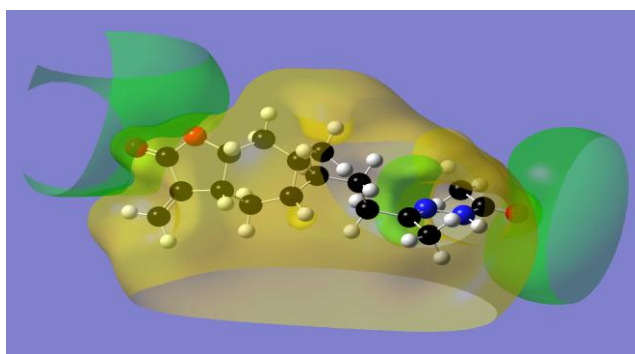


Figure 4. MEP map of molecule 1.

The green isovalue surface corresponds to negative MEP values (-0.01) and the yellow isovalue surface to positive MEP values (0.01).

We can see that in this extended conformer most of the molecule is surrounded by a positive MEP region. Negative MEP regions are observed around the oxygen atoms in ring A and around the nitrogen and oxygen atoms of the side chain connected to ring C (Fig. 2).

***In vitro* antifungal activity against *B. cinerea*.**

The associated statistical parameters of Eq. 2 show that this equation is statistically significant and that the variation of a group of six local atomic reactivity indices belonging to the common skeleton (Fig. 2) explains about 86% of the variation of the *in vitro* antifungal activity against *B. cinerea*. Fig. 5 shows the plot of predicted vs. observed $\log(\text{IC}_{50})$ values.

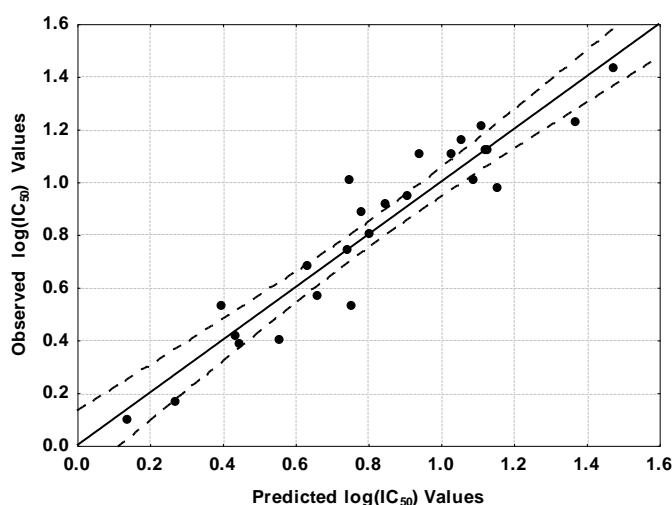


Figure 5. Plot of predicted vs. observed $\log(\text{IC}_{50})$ values (Eq. 2). Dashed lines denote the 95% confidence interval.

We can see that very few points lie relatively far from the 95% confidence interval. Therefore and in a first approach the common skeleton hypothesis seems to work well for this case. We cannot exclude the possibility that one or more molecules have extra interactions through atoms that are not included in the common skeleton. The beta values (not shown) indicate that the relative importance of these indices is $F_{11}(\text{LUMO})^* > \omega_{12} > F_3(\text{HOMO}-1)^* > S_{15}^N = S_{14}^N(\text{LUMO}+1)^* > F_{15}(\text{HOMO}-2)^*$ (see Fig. 2). High antifungal activity is then associated with high values for $F_{11}(\text{LUMO})^*$, $F_3(\text{HOMO}-1)^*$, $F_{15}(\text{HOMO}-2)^*$ and ω_{12} , and with small values for S_{15}^N and $S_{14}^N(\text{LUMO}+1)^*$. In the case of atom 11, $(\text{LUMO})_{11}^*$ is of σ nature. It is suggested that this atom interacts with a σ electron-rich center through its lowest vacant orbital (see Fig. 2 for atom numbers). As an example of moieties having a σ electronic structure we may cite the methylene chains. Nitrogen 12 seems to act as an electron acceptor but the nature of this interaction cannot be elucidated because the atomic electrophilicity is a number not depending on a particular MO. Atom 3, with only σ MOs localized on it, seems to participate in an interaction with a σ electron-deficient center through its two highest occupied MOs. Oxygen 15 also interacts with an electron-deficient center but through its three highest occupied MOs. A low value for S_{15}^N indicates that atom 15 should act as a bad electron acceptor, a fact that is consistent with the requirement for $F_{15}(\text{HOMO}-2)^*$. A low value for $S_{14}^N(\text{LUMO}+1)^*$, a σ MO, could be an indication that atom 14 interacts with an occupied σ MO only through its lowest vacant MO. Maybe $(\text{LUMO}+1)_{14}^*$ participates in a repulsive interaction with a σ vacant MO localized on the partner. All these ideas are presented in the two-dimensional (2D) partial inhibition pharmacophore shown in Fig. 6.

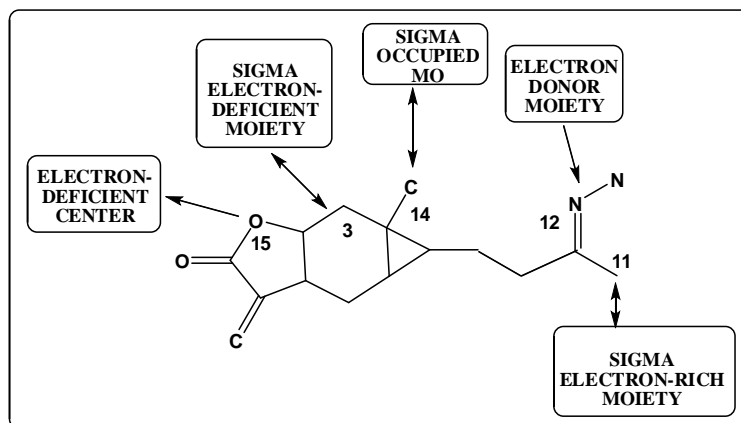


Figure 6. Partial 2D inhibition pharmacophore for the *in vitro* antifungal activity against *B. cinerea*.

Note the important fact that the proposed interactions for atoms 3, 11 and 14 are fully consistent with the positive structure of the MEP map shown in Fig. 4.

In vitro antifungal activity against *C. lagenarium*.

The associated statistical parameters of Eq. 3 show that this equation is statistically significant and that the variation of a group of six local atomic reactivity indices belonging to the common skeleton explains about 91% of the variation of the *in vitro* antifungal activity against *C. lagenarium*. Fig. 7 shows the plot of predicted vs. observed $\log(\text{IC}_{50})$ values.

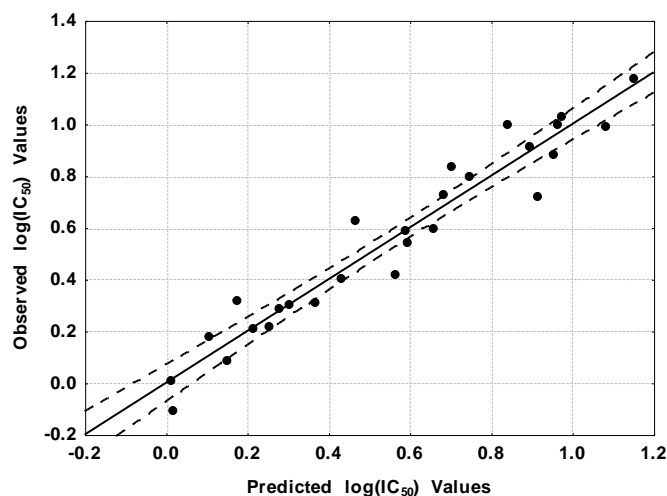


Figure 7. Plot of predicted vs. observed $\log(\text{IC}_{50})$ values (Eq. 3). Dashed lines denote the 95% confidence interval.

We can see that few points lie relatively far from the 95% confidence interval. Then the common skeleton hypothesis seems to work well also for this case. The beta values (not shown) indicate that the relative importance of these indices is $F_8(\text{LUMO}+1)^* > \omega_{12} = F_{11}(\text{HOMO}-2)^* > F_9(\text{LUMO}+1)^* = S_{18}^E(\text{HOMO}-1)^* > F_{10}(\text{LUMO}+2)^*$ (see Fig. 2). Potent antifungal activity is then associated with high values for $F_8(\text{LUMO}+1)^*$, $F_9(\text{LUMO}+1)^*$, $S_{18}^E(\text{HOMO}-1)^*$, ω_{12} and $F_{10}(\text{LUMO}+2)^*$, with small values for $F_{11}(\text{HOMO}-2)^*$. A high value of $S_{18}^E(\text{HOMO}-1)^*$ is related with optimal activity. Carbon 18 acts by interacting with an electron-deficient center through its first two highest occupied MOs. The C11 carbon of the methyl group has only σ MOs localized on it. A low value for $F_{11}(\text{HOMO}-2)^*$ could be an indication of a repulsive interaction between the $\sigma(\text{HOMO}-2)_{11}^*$ and σ MOs localized on the partner. A high

value for ω_{12} suggests that nitrogen 12 seems to act as an electron acceptor as in the previous case. High values for $F_8(LUMO+1)^*$ and $F_9(LUMO+1)^*$, both of σ nature, suggests that atoms 8 and 9 are interacting with an electron-rich moiety (probably of σ nature) through their two lowest vacant MOs. Carbon atom 10 seems to interact with an electron-rich center through its first three lowest vacant MOs. This interaction is probably of π - π stacking type. All these suggestions are presented in the 2D partial inhibition pharmacophore shown in Fig. 8.

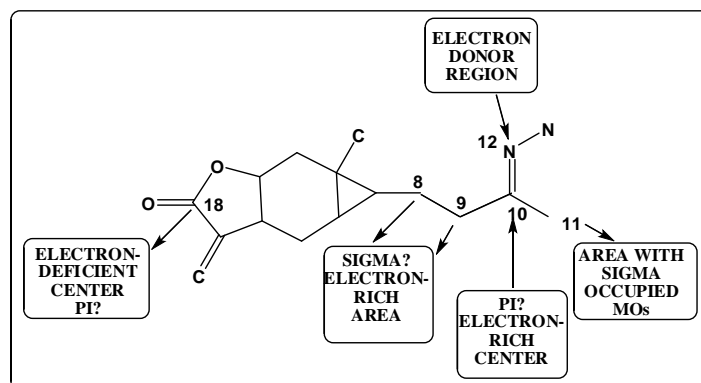


Figure 8. Partial 2D inhibition pharmacophore for the *in vitro* antifungal activity against *C. lagenarium*.

In vivo antifungal activity against *B. cinerea*.

The associated statistical parameters of Eq. 4 show that this equation is statistically significant and that the variation of a group of seven local atomic reactivity indices belonging to the common skeleton explains about 85% of the variation of the *in vivo* antifungal activity against *B. cinerea*. Figure 9 displays the plot of predicted vs. observed $\log(IC_{50})$ values.

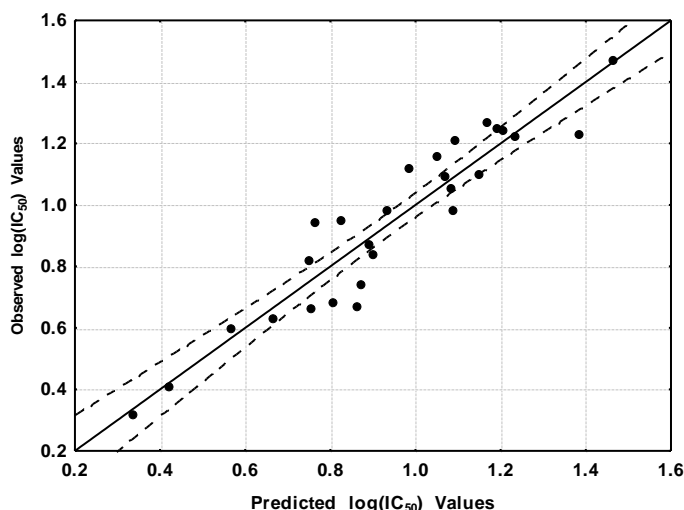


Figure 9. Plot of predicted vs. observed $\log(IC_{50})$ values (Eq. 4). Dashed lines denote the 95% confidence interval.

We can see that a small number of points lie relatively far from the 95% confidence interval. In this case the common skeleton hypothesis seems to perform well. The beta values (not shown) indicate that the relative importance of these indices is $\omega_{12} > F_{11}(HOMO)^* > S_3^E(HOMO-2)^* \gg Q_7^{\max} > S_3^N = F_{14}(LUMO+2)^* > S_{15}^E(HOMO-1)^*$ (Fig. 2). High antifungal activity is then associated with high values for $F_{11}(HOMO)^*$, ω_{12} , Q_7^{\max} and S_3^N , and with small values for $S_3^E(HOMO-2)^*$, $F_{14}(LUMO+2)^*$ and $S_{15}^E(HOMO-1)^*$. A high value for the electrophilicity of nitrogen 12 indicates that this atom is interacting with an electron-donor center. A high value for $F_{11}(HOMO)^*$ is required.

$(\text{HOMO})_{11}^*$ is a σ MO. It is suggested that atom 11 is interacting with a region of empty σ MOs. A high value for Q_7^{max} indicates that atom 7 could be involved in an electrostatic interaction with a negatively charged moiety. A high value for S_3^N is associated with optimal activity. Given that all MOs localized on atom 3 are of σ nature and that the total atomic nucleophilic superdelocalizability is indicative of electron-acceptor capacity we suggest that atom 3 is interacting with an electron cloud, also probably of σ nature. A small value for $S_3^E(\text{HOMO}-2)^*$ is consistent with the suggestion of a repulsive interaction of this σ MO with another σ cloud. A small value for $F_{14}(\text{LUMO}+2)^*$ is needed. As all MOs of atom 14 are of σ nature, it is suggested that atom 14 is interacting with occupied MOs (σ) through its two lowest vacant MOs and that its third lowest vacant MO is engaged in a repulsive interaction, probably with an empty σ MO. A low value for $S_{15}^E(\text{HOMO}-1)^*$ suggests that oxygen 15 is interacting with an electron-deficient center through its HOMO* but its (HOMO-1)* is engaged in a repulsive interaction with an occupied MO. All these proposals are presented in the 2D partial inhibition pharmacophore shown in Fig. 10.

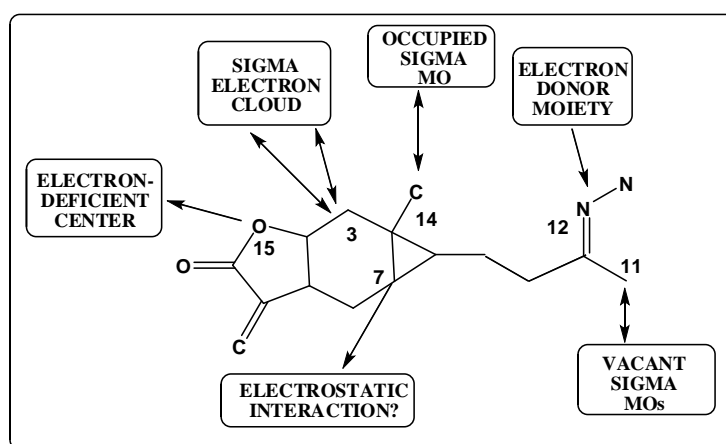


Figure 10. Partial 2D inhibition pharmacophore for the *in vivo* antifungal activity against *B. cinerea*.

We can see that the results for the *in vitro* and *in vivo* antifungal activity against *B. cinerea* are similar but not the same, explaining the correlation of only 72% of the measured data. The corresponding pharmacophores (Figs. 6 and 10) show differences at atoms 3 and 11. In the light of these results, the antifungal action mechanisms seem to be different. It is highly probable that in the case of the *in vivo* data the molecules are involved in one or more extra steps. In any case it is the *in vivo* data and the structure-activity relationships derived from them that must be considered for the development of more potent fungicides.

CONCLUSIONS

With the use of a formal method we obtained solid results relating electronic structure with antifungal activity measured *in vivo* and *in vitro*. The hypothesis of a common skeleton encoding most of the variation of the activity is established. The *in vivo* and *in vitro* action mechanisms seem to be different. The method employed here can treat the participation of σ MOs quite well. A good correlation appears to exist between the molecular electrostatic potential spatial structure and the local atomic reactivity indices appearing in the results.

ACKNOWLEDGEMENTS

Mr. S. Romero is thanked for helping to prepare the initial molecular geometries.

REFERENCES

- [1]. H Minato; S Nosaka; I Horibe, *J. Chem. Soc. (Res.)*, 1964, 5503-5510.
- [2]. H Minato; I Horibe, *Chem. Comm.*, 1967, 358-360.
- [3]. H Minato; I Horibe, *J. Chem. Soc. C: Org.*, 1968, 2131-2137.

- [4]. TR Hoye; JR Vyvyan, *J. Org. Chem.*, 1995, 60, 4184-4195.
- [5]. M Holub; Z Samek; J Toman, *Phytochem*, 1972, 11, 2627-2628.
- [6]. F Bohlmann; LN Misra; J Jakupovic, *Phytochem*, 1985, 24, 1021-1026.
- [7]. J-T Feng; Z-Q Ma; J-H Li; J He; H Xu; X Zhang, *Molecules*, 2010, 15, 6485-6492.
- [8]. J-T Feng; H Wang; S-X Ren; J He; Y Liu; X Zhang, *J. Agr. Food Chem.*, 2012, 60, 3817-3823.
- [9]. H Wang; S-X Ren; Z-Y He; D-L Wang; X-N Yan, et al., *Int. J. Mol. Sci.*, 2014, 15, 4257-4272.
- [10]. JS Gómez-Jeria, *Boll. Chim. Farmac.*, 1982, 121, 619-625.
- [11]. JS Gómez-Jeria, *Int. J. Quant. Chem.*, 1983, 23, 1969-1972.
- [12]. JS Gómez-Jeria, "Modeling the Drug-Receptor Interaction in Quantum Pharmacology," in *Molecules in Physics, Chemistry, and Biology*, J. Maruani Ed., vol. 4, pp. 215-231, Springer Netherlands, 1989.
- [13]. JS Gómez-Jeria; M Ojeda-Vergara; C Donoso-Espinoza, *Mol. Engn.*, 1995, 5, 391-401.
- [14]. JS Gómez-Jeria; M Ojeda-Vergara, *J. Chil. Chem. Soc.*, 2003, 48, 119-124.
- [15]. JS Gómez-Jeria, *Elements of Molecular Electronic Pharmacology (in Spanish)*, Ediciones Sokar, Santiago de Chile, 2013.
- [16]. JS Gómez-Jeria, *Canad. Chem. Trans.*, 2013, 1, 25-55.
- [17]. JS Gómez-Jeria; M Flores-Catalán, *Canad. Chem. Trans.*, 2013, 1, 215-237.
- [18]. A Paz de la Vega; DA Alarcón; JS Gómez-Jeria, *J. Chil. Chem. Soc.*, 2013, 58, 1842-1851.
- [19]. I Reyes-Díaz; JS Gómez-Jeria, *J. Comput. Methods Drug Des.*, 2013, 3, 11-21.
- [20]. JS Gómez-Jeria; DR Morales-Lagos, *J. Pharm. Sci.*, 1984, 73, 1725-1728.
- [21]. JS Gómez-Jeria; D Morales-Lagos; JI Rodríguez-Gatica; JC Saavedra-Aguilar, *Int. J. Quant. Chem.*, 1985, 28, 421-428.
- [22]. JS Gómez-Jeria; P Sotomayor, *J. Mol. Struct. (Theochem)*, 1988, 166, 493-498.
- [23]. JS Gómez-Jeria; M Ojeda-Vergara, *Int. J. Quant. Chem.*, 1997, 61, 997-1002.
- [24]. JS Gómez-Jeria; L Lagos-Arancibia, *Int. J. Quant. Chem.*, 1999, 71, 505-511.
- [25]. F Soto-Morales; JS Gómez-Jeria, *J. Chil. Chem. Soc.*, 2007, 52, 1214-1219.
- [26]. DA Alarcón; F Gatica-Díaz; JS Gómez-Jeria, *J. Chil. Chem. Soc.*, 2013, 58, 1651-1659.
- [27]. JS Gómez-Jeria, *Int. Res. J. Pure App. Chem.*, 2014, 4, 270-291.
- [28]. JS Gómez-Jeria, *Der Pharm. Lett.*, 2014, 6., 95-104.
- [29]. JS Gómez-Jeria, *Brit. Microbiol. Res. J.*, 2014, 4, 968-987.
- [30]. JS Gómez-Jeria, *SOP Trans. Phys. Chem.*, 2014, 1, 10-28.
- [31]. JS Gómez-Jeria, *Der Pharma Chem.*, 2014, 6, 64-77.
- [32]. JS Gómez-Jeria, *Res. J. Pharmac. Biol. Chem. Sci.*, 2014, 5, 2124-2142.
- [33]. D Muñoz-Gacitúa; JS Gómez-Jeria, *J. Comput. Methods Drug Des.*, 2014, 4, 33-47.
- [34]. D Muñoz-Gacitúa; JS Gómez-Jeria, *J. Comput. Methods Drug Des.*, 2014, 4, 48-63.
- [35]. DI Pino-Ramírez; JS Gómez-Jeria, *Amer. Chem. Sci. J.*, 2014, 4, 554-575.
- [36]. F Salgado-Valdés; JS Gómez-Jeria, *J. Quant. Chem.*, 2014, 2014 Article ID 431432, 1-15.
- [37]. R Solís-Gutiérrez; JS Gómez-Jeria, *Res. J. Pharmac. Biol. Chem. Sci.*, 2014, 5, 1401-1416.
- [38]. MS Leal; A Robles-Navarro; JS Gómez-Jeria, *Der Pharm. Lett.*, 2015, 7, 54-66.
- [39]. JS Gómez-Jeria; A Robles-Navarro, *Res. J. Pharmac. Biol. Chem. Sci.*, 2015, 6, 1811-1841.
- [40]. JS Gómez-Jeria; A Robles-Navarro, *Res. J. Pharmac. Biol. Chem. Sci.*, 2015, 6, 755-783.
- [41]. JS Gómez-Jeria; A Robles-Navarro, *Der Pharma Chem.*, 2015, 7, 243-269.
- [42]. JS Gómez-Jeria; A Robles-Navarro, *Res. J. Pharmac. Biol. Chem. Sci.*, 2015, 6, 1337-1351.
- [43]. MJ Frisch; GW Trucks; HB Schlegel; GE Scuseria; MA Robb, et al., G03 Rev. E.01, Gaussian, Pittsburgh, PA, USA, 2007.
- [44]. JS Gómez-Jeria, *J. Chil. Chem. Soc.*, 2009, 54, 482-485.
- [45]. Statsoft, Statistica 8.0, 2300 East 14 th St. Tulsa, OK 74104, USA, 1984-2007.
- [46]. Chemaxon, MarvinView, www.chemaxon.com, USA, 2014.
- [47]. RD Dennington; TA Keith; JM Millam, GaussView 5.0.8, GaussView 5.0.8, 340 Quinnipiac St., Bldg. 40, Wallingford, CT 06492, USA, 2000-2008.